Investigation of an Actively Cooled Leading Edge for Hypersonic Ramjet Engines

STEPHEN E. GRENLESKI* AND FREDERICK S. BILLIG†
Applied Physics Laboratory, The Johns Hopkins University, Silver Spring, Md.

This report examines the engineering problems associated with the design of a water-cooled, tubular nickel leading edge for a hypersonic inlet. Small leading-edge radii (0.015–0.035 in.) were considered in order to minimize the distortion to the inlet flowfield. A design analysis was performed for conditions which could be obtained in the Applied Physics Laboratory (APL) arc-driven wind tunnel, viz., Mach 6.5, total temperature 5400°R, total pressure, 450 psia. Experiments on an 0.0255-in.-radius leading edge at these conditions showed that the integrity of the tube could be maintained even though the tube was deformed by small particles in the stream. Using moderate coolant velocities the calculated outer wall temperature at the stagnation point was 800°R, and the combined thermal and pressure stresses were found to be 24% of the elastic limit. Selected results of a more generalized study of the application of actively cooled leading edges for hypersonic vehicles are also discussed. The fabrication techniques used to join nickel tubes with electrodeposited nickel and to form a composite leading-edge structure for a second series of tests are described. Photomicrographs show that a bond of one-grain-boundary thickness can be achieved. Both single-tube and composite structures were tested at Mach 3.13 with stagnation conditions of 4440°R and 435 psia, giving 2.1 times the heating rate at the stagnation point attained with the Mach 6.5 tests. Assuming Newtonian flow and the Detra and Hidalgo correlation modified for a cylinder in cross flow, the estimated heat transfer to the leading edge was found to be 73% of the measured value.

Nomenclature

A = area
D = diameter
f = friction factor
h = enthalpy
k = shape factor
L = length
M = Mach number
p = pressure
q = heat-transfer rate, dynamic pressure
R = radius
t = thickness
T = temperature
V = velocity
x, y = axial and normal coordinate, respectively
Z = altitude
δ = wedge angle
Δ = shock wave standoff distance
Δp = pressure drop
ρ = density
θ = shock angle

Subscripts

c = curvature
cond = conduction
conv = convection
f = film
H_2O = bulk water condition
i, w = inside and outside wall condition, respectively
liq, sat = mixed outlet and saturation condition, respectively
$0, r, t$ = freestream, recovery, and total condition, respectively
rad = radiation
s = stagnation point
sl = sea level conditions
1, 2, 3 = first-, second-, and third-wedge compression region, respectively

Received June 20, 1967. This work was supported by NASA Office of Aeronautical Research, Advanced Research and Technology under Contract NOw 62-0604-c with the Department of the Navy. The authors wish to acknowledge R. E. Wilson (Naval Ordnance Laboratory and University of Maryland) for his supervision of the analytical portion and Mach 6.46 wind-tunnel blockage tests that were used by S. E. Grenleski for a Master of Science thesis in Aeronautical Engineering at the University of Maryland. Also, acknowledgment is due R. Allen and J. Funk of the Applied Physics Laboratory for their assistance during this program. Thanks are due to J. VanNoy for typing the report.

* Senior Engineer, Hypersonic Propulsion Group.
† Project Supervisor, Hypersonic Propulsion Group. Associate Fellow AIAA.

Introduction

ONE of the more critical problem areas in the development of air-breathing engines for hypersonic flight is the leading-edge structure of the inlet compression surface. In this region not only must the maximum heating rates be tolerated but distortions to the flowfield caused by excessive blunting and/or thermal warping of compression surface must be held to a minimum if high inlet performance is to be achieved. For most of the attractive hypersonic missions the freestream dynamic pressure, q_0 is sufficiently high so that the beneficial effects of radiation are inconsequential in cooling stagnation regions. Moreover, slender relatively sharp shapes are customary, so relief by heat conduction away from the hottest regions is relatively small. Thus, the design of the uncooled structure must contend with surface temperatures approximately equal to the stagnation temperature at the leading edge and the laminar recovery temperature T_r in the immediate downstream region.

The use of conventional high-temperature materials, e.g., stainless steel, nickel, and cobalt-based alloys, is limited to about Mach 5 where the stagnation temperature T_{t_0} in the tropopause is 2290°R and T_r = 1965°R. Uncooled refractory materials will have some utility at low hypersonic speeds, possibly Mach 8, $T_r \approx$ 3865°R to Mach 10, $T_r \approx$ 5480°R depending on the severity of the surface oxidation.

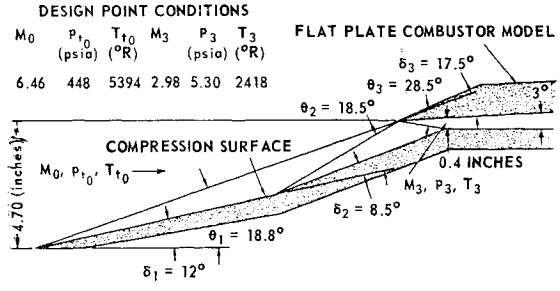

Fig. 1 Two-dimensional ramjet inlet-combustor model for hypersonic combustion testing.

Studies in the literature include that of Bowers,[1] who evaluated thin shell edge structures fabricated from coated molybdenum alloys for the Dyna-Soar glide vehicle. Although the strength of the structures was adequate, oxidation failure through the disilicide coatings occurred during radiant heating and plasmajet temperature simulation tests. Scala and Nolan[2] made analytical studies of the transient heat transfer and surface oxidation rates for glide vehicle reentry trajectories using representative properties of both conventional and pyrolytic graphite. They conclude that graphite could be used successfully for high-temperature leading edges, if the regression of the leading edge can be tolerated. Of course, only a very limited amount of leading-edge regression can be sustained in the inlet compression surface before significant distortions to the flowfield would be encountered. Moreover, coated molybdenum and pyrolytic graphite are both relatively expensive and would require complicated methods of attachment to the downstream structure. Thus, it appears that either actively or transpirationally cooled leading-edge structures will become of interest even in the low hypersonic range.

This paper investigates the engineering problems pertinent to the design and fabrication of an actively cooled nickel leading-edge tube. The analytical studies include calculations of cooling requirements for structural adequacy for leading-edge radii from 0.015 to 0.035 in., a description of detached shock position and shape for a 0.0255-in. radius, and a more generalized analysis of water-cooled leading-edge structures. The experimental work was carried out in two phases. In the first phase, single water-cooled tubes were attached to a simple two-dimensional ramjet model and tested in the Mach 6.5 arc-driven hypersonic wind tunnel at the APL to verify the concept. The second phase includes a description of the fabrication technique used to connect several nickel tubes to a nickel forebody by means of electroplating and subsequent machining of the assembly. Verification of a high-quality plating interface was obtained by photomicrographs, and an approximate method of estimating leading-edge heat-transfer rate was checked by direct measurements in an arc-driven wind tunnel, using a lower Mach number freejet apparatus which is more convenient to obtain measurements and also provides a more severe heat-transfer environment.

Analytical Studies

The simple two-dimensional ramjet inlet-combustor wind-tunnel model as shown in Fig. 1 is being considered for hypersonic testing of an integrated supersonic combustion engine. The model is 6 in. wide and consists of a compression surface, a cowl, and main body plus miscellaneous mounting struts. The compression is accomplished through two oblique shocks on the ramp plus a reflected shock from the cowl. The intent is to place the cowl at the intersection of the two oblique shocks and have the cowl-reflected shock strike the knee of the compression ramp to prevent over compression and/or undesirable expansions.

The design was based on the test conditions available in the 15-in.-diam d.c. arc-heated wind tunnel at the APL. Pitot pressure surveys of the tunnel flowfield showed that the tunnel Mach number was 6.5 ± 0.1 based on equilibrium nozzle expansion[3] from plenum conditions of 450 psia and 5400°R. The tunnel static pressure at this condition is 0.095 psia simulating 112,000 ft, but the static temperature is 698°R or 260°R above the temperature corresponding to that altitude. Stagnation-point heating is simulated by matching pitot pressure and total enthalpy so that the unrealistic temperature just implies simulation at a somewhat higher Mach number and altitude. In this case, these conditions are $M_0 = 8$, $Z = 145$ kft.

The heat transfer to the stagnation point on the compression surface was examined using the Detra and Hidalgo[4] correlation

$$\frac{q_s}{A} = 3600 \cdot 865 \cdot 2^{(k-1)/2} \left(\frac{V_0}{10^4}\right)^{3.15} \left(\frac{\rho_0}{\rho_{sl}}\right)^{0.5} \frac{h_t - h_w}{h_t - h_{w300}} \quad (1)$$

which has been modified to include the term $2^{(k-1)/2}$, where $k = 1$ for axisymmetric flow and $k = 0$ for two-dimensional flow such as discussed herein. This correlation is presumably accurate to 10% over the range of $6000 \leq V_0 \leq 26{,}000$ fps and $8 \times 10^{-5} \leq \rho_0/\rho_{sl} < 1$. Included in the determination of this expression is the consideration of a Newtonian velocity gradient at the stagnation point, Avco gas dynamic charts for equilibrium air, the viscosity-temperature dependence given by Sutherland, a Lewis number of 1.4, and a Prandtl number of 0.71.

The stagnation-point heat flux was calculated as a function of wall temperature for the tunnel conditions and the results plotted in Fig. 2. Note that the equilibrium wall temperature for an uncooled leading edge with the radius chosen (0.025 in.) is approximately 4400°R. In subsequent calculations the method of Lees[5] was used to compute the heat-transfer-rate distribution about the cylindrical body with its axis normal to the airstream. Although the heat flux for the complete range of possible wall temperatures is shown, in fact, the study revealed that only a limited range of outside wall temperatures, viz., 600–1000°R are consistent with the concept of thin walls and moderate stress levels.

The method of cooling the model is to force coolant through a network of small diameter holes. Water was chosen because of its attractive properties, but other coolants, e.g., liquid hydrogen, are feasible. The composite structure consists of a base structure containing drilled holes joined to an electrodeposited leading-edge section. The limitations

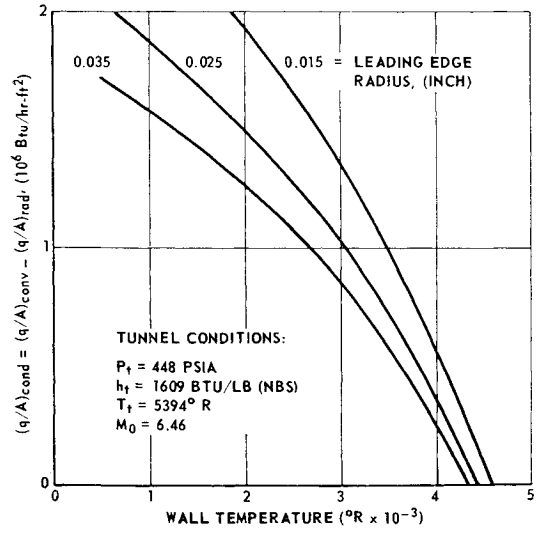

Fig. 2 Calculated stagnation-point heat flux vs wall temperature and leading-edge radius ($\epsilon = 0.7$).

on the extension of the drilled structure to a minimum section thickness are the drill diameter and the drill runout, which varies inversely with the drill diameter. In this case, the smallest successfully drilled hole, of 6-in. depth, using conventional methods was 0.093 in. in diameter with 0.006 to 0.012-in. runout. Rather than extending the drilled section to the theoretical limit, thus compounding the fabrication problems, the minimum thickness was held to 0.224 in., and it was necessary to devise a different method of fabrication to obtain a leading edge with acceptable bluntness.

The leading-edge design that was conceived consisted of an assembly of several separately cooled tubes in which each succeeding tube is downstream and in line with the preceding tube as seen in Fig. 3. The method of fabricating the tube assembly involves the electrodeposition of metal about tubes held in an assembly jig. The plated metal holds the tubes together and provides excess material which can be machined to a variety of desired final shapes. This leading-edge assembly can then be either brazed or mechanically attached to the drilled model plate. Two of the desirable features of the structure are that in the event of failure of the leading edge tube the adjacent tube would serve as the leading edge, as shown in the experimental results section, and that a damaged leading-edge assembly could be salvaged by replacing only the damaged tube.

Several materials were considered for the leading edge. The selection was a compromise among the properties listed in Table 1 and the electroplating characteristics of the metals. Since it was desirable to run many tests with this model, a hard metal was suggested to assure the capability of withstanding abrasion caused by contaminents in the airstream. Metal hardness is seen to increase from 30 to 153 Brinell as the thermal conductivity decreases from 242 to 9 Btu/hr-ft^2-°F/ft for silver and 304 stainless steel, respectively. Although stainless steel is the hardest material considered, electrodeposition is considerably more difficult than with the pure metals. Nickel with a thermal conductivity of 54 Btu/hr-ft^2-°F/ft, a Brinell hardness of 105 and excellent electrodeposition characteristics appeared to be the most logical choice and was, therefore, selected for the design.

The design was based on the use of standard stock tubing made of Ni 270, a high-purity material,[7] having an outside diameter of 0.051 in. and an inside diameter of 0.041 in. Using these dimensions and the one-dimensional heat-conduction expression, values of the inside wall temperature T_i were calculated as a function of the outside wall temperatures at the stagnation point. The most critical design point occurs at the downstream end of the tube where the maximum inner wall temperature would be 325°F and $q_{cond}/A = 1.96 \times 10^6$ Btu/hr-ft^2 for an outer wall temperature $T_w = 340$°F. For these conditions the local water pressure must be maintained at a minimum of 97 psia, which is the saturation pressure, to prevent the possibility of film boiling burnout.

To calculate the heat load for the leading-edge tube an estimated additional 6 in. of length is assumed to be required for connecting to the protected larger diameter water-supply and return lines thus giving an over-all length of 12 in. of 0.051-in.-diam tubing exposed to the air flowing through the tunnel. This assumption could be regarded as a safety factor, in that part of the extension line could be curved and placed parallel to the airstream downstream of the leading edge and therefore not receive as much heating.

Table 1 Comparison of thermal conductivity and Brinell hardness of metals considered for leading-edge tube

Metal	Thermal conductivity,[6, 7] Btu/hr-ft^2-°F/ft	Brinell hardness[6]
Silver	242	30
Copper	211	40
Aluminum	101	49
Nickel 270	54	105
304 stainless steel	9	153

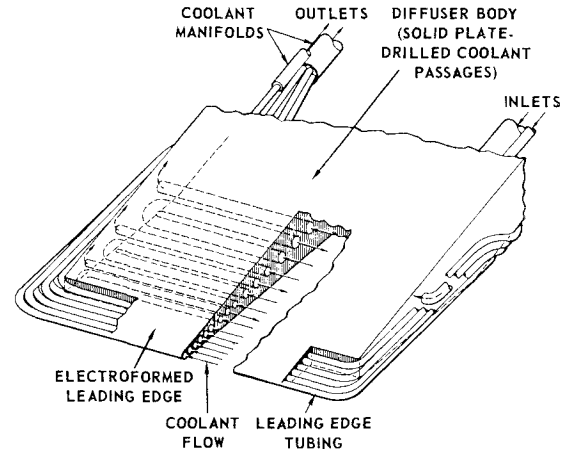

Fig. 3 Schematic of electrodeposited nickel leading-edge structure attached to larger compression surface.

Using the method suggested in Ref. 5 for the distribution of q_{cond}/A, the mean q on the rounded forward surface is 2.17 Btu/sec. For the rear part of the tube it is assumed that the heat that must be carried away by the water enters from the two outer flat surfaces of the shaded areas shown in Fig. 4 at the rates prevailing 78° and 90° from the stagnation point. Thus, the total q to the leading-edge tube is 2.53 Btu/sec. To determine the required velocity of the coolant water it is necessary to consider both the heating capacity and the heat-transfer coefficient of the fluid. For small diameter tubes operating in a relatively modest environment, the heat capacity is generally the design constraint. In this case, assuming that the entering temperature of the coolant is 60°F and the exit temperature is 180°F, again conservative, a water velocity of 36.9 fps is required. With this velocity the flow in the tube would be turbulent and the water side heat-transfer coefficient would be sufficiently large to provide the previously calculated T_i. The only remaining requirements were to see if the pressure drop and stress levels were not excessive.

Using the Darcy equation (Ref. 8, Sec. 3, pp. 247–250) which was subsequently checked experimentally to about 10% (see Fig. 5), the pressure drop was calculated to be about 62 psia for water at a temperature of 180°F. The available water-supply pressure is 265 psia which provides a margin of safety over the calculated pressure drop and saturation pressure required.

The combined stresses in the tube were calculated as the algebraic sum of the pressure and thermal stresses. The thermal stresses, compressive at the inner radius and tensile at the outer radius, were calculated using the equations for elastic deformation given by Timoshenko.[9] The important thermal stress is a tensile stress of 2440 psi at the outer radius,

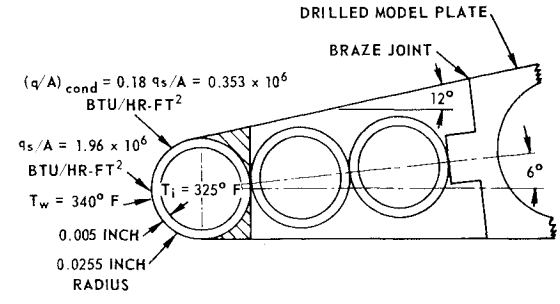

Fig. 4 Sketch showing heat-transfer surface for leading-edge tube.

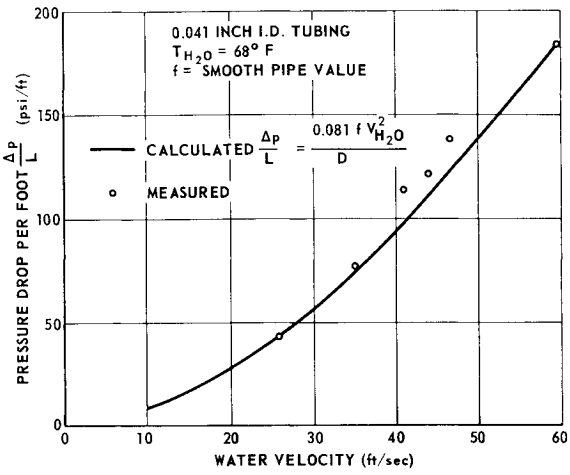

Fig. 5 Pressure drop per foot vs water velocity.

which when added to the pressure stress gives a combined stress of 3090 psi. Since the yield strength of the material is 13,000 psi, it is apparent that the stress can be tolerated.

Since the wedge surface has a finite bluntness, the initial shock wave becomes detached from the body with a small but finite portion of the flow negotiating a much stronger compression. The shape of the wave has been experimentally observed[10] to approximate a hyperbola, which becomes asymptotic to an attached oblique wave at a point some distance from the surface as shown in Fig. 6. Billig[11] presents a simplified method of computing the shape of the detached hyperbolic shock wave. He correlated experimental shock wave data into an empirical expression for the shock radius of curvature at the stagnation point. For the two-dimensional wedge flow considered here, the radius of curvature R_c,

$$R_c/R = 1.386 \exp[1.8/(M - 1)^{0.75}] \quad (2)$$

is given in Eq. (2). The equation for the coordinates of the hyperbolic shock shape is

$$x = R + \Delta - R_c \cot^2\theta \left[\left(1 + \frac{y^2 \tan^2\theta}{R_c^2}\right)^{1/2} - 1\right] \quad (3)$$

The shock-wave standoff distance Δ is computed from the Ambrosio and Wortman[12] correlation of experimental results and is given as

$$\Delta/R = 0.386 \exp(4.67/M^2) \quad (4)$$

for wedge flow. For the example case, $R = 0.0255$ in., the shock standoff distance Δ is 0.011 in. and the vertex radius of curvature R_c is 0.059 in. The wave becomes asymptotic to within 0.5° of the oblique shock angle at a point 0.95 in. from the model axis and 2.29 in. downstream. By the time the shock has reached the cowl lip, its position is essentially

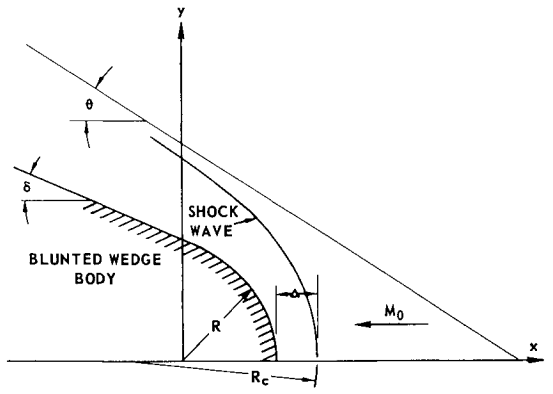

Fig. 6 Schematic of detached shock wave.

coincident with that of an equivalent attached wave. Assuming that the additional compression in the innermost stream tubes is subsequently lost in undesirable expansion, the mass weighted total pressure loss is 4% due to the blunting. By comparison, if instead the leading-edge bluntness had to be increased to 0.052-in. radius, equal to the smallest drilled hole radius plus a wall of 0.005 in., then the total pressure loss would be 8%.

Before discussing the experimental verification of the design principles, some of the results of a more general parametric study of the application of active cooling leading edges will be given. Figure 7 shows the limiting length of a single pass of water-cooled Ni 270 tubing as a function of flight Mach number. The following design constraints were selected: 1) maximum temperature rise in the coolant, 150°F; 2) maximum pressure drop in the coolant passage, 2000 psia based on constant friction factor of 0.022; 3) maximum stress in the tubing 13,000 psia.

Families of curves are shown for leading-edge radii of 2×10^{-3} ft (24 mils) and 2×10^{-2} ft for $q_0 = 500$ psia, a reasonable value of dynamic pressure for a high-altitude hypersonic vehicle. Calculations were made for radius-to-wall-thickness ratios (R/t) of 48, 12, 4.8, and 2.4 for the large radius tube, whereas in the smaller tube calculation the largest value was eliminated because it results in an unreasonably thin structure.

For each tube geometry the coolant velocity selected was based on maximizing the length of tubing with the constraint that the velocity was at least sufficient to prevent tube burnout as governed by either the Gunther[13] correlation for boiling heat transfer,

$$(q/A)_{\text{burnout}} = 0.0135\, V^{0.5}(T_{\text{sat}} - T_{\text{liq}}) \quad (5)$$

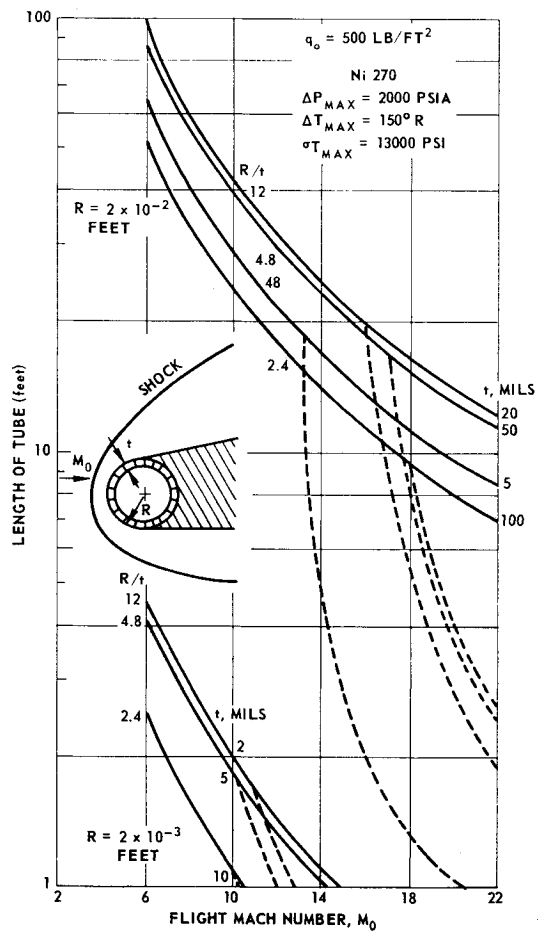

Fig. 7 Maximum length of a single pass, water-cooled, leading-edge tube.

or the more conservative turbulent flow relationship given by Marks (Ref. 8, Sec. 4, p. 372),

$$q/A = 160(1 + 0.012\ T_f)V^{0.8}(T_i - T_{liq})/D^{0.2} \quad (6)$$

The analysis showed for the cases studied the optimum water velocity (dictated by the heat-capacity constraint) would always be greater than that for boiling burnout (solid curves) but would be below the required turbulent velocity at high Mach numbers (dashed curves). Therefore if the design were based on the more conservative relationship, i.e., Eq. (6), the heat-transfer coefficient would constrain and the temperature rise in the coolant would be less than 150°F.

The solid curves represent systems in which the velocity is increased to the point where the pressure drop forces an initial pressure equal to that producing the maximum tolerable stress level, but not exceeding 2000 psi. Two competing factors lead to the optimum wall thickness of approximately 0.020 in. in the $R = 2 \times 10^{-2}$ ft curves. As the wall thickness decreases, the pressure drop per unit length decreases at a given velocity, but, in turn, the permissible maximum pressure also decreases due to the stress limit. For the smaller diameter tube this optimum would again exist but at wall thickness less than 2 mils, which would be unreasonably thin.

Additional calculations with substitute materials having higher permissible stress levels showed that only small length increases could be obtained before the maximum pressure drop limit would be reached. From this figure it may be concluded that for a long pass heat exchanger, a large diameter is desirable, but of course this leads to more severe blunting problems and at the same times requires much larger pumping capacity. In any case, lengths of the order of 1–100 ft seem quite reasonable for practical cooling systems.

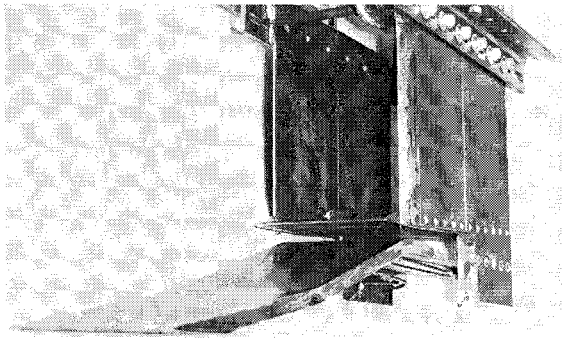

a) View looking downstream

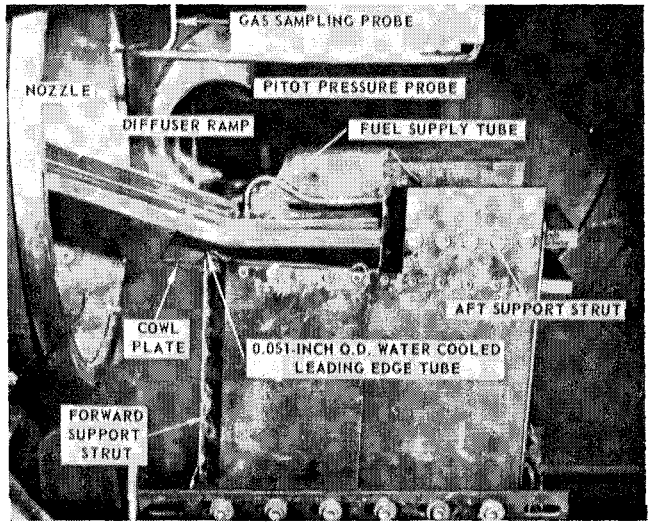

b) Mounted model in APL arc-driven hypersonic tunnel

Fig. 8 Two-dimensional "boiler-plate" model of inlet-combustor for blockage tests at $M_0 = 6.46$.

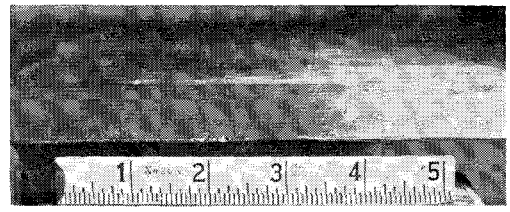

a) View showing deformation sustained without failure

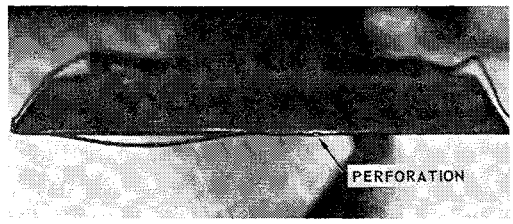

b) View showing perforation in tube; water flow inside tube from right to left

Fig. 9 Downstream view of 0.025-in.-radius leading edges after tests at Mach 6.46.

Experimental Work

Prior to the fabrication of a completely cooled inlet-combustor model, an inexpensive heat sink "boiler plate" blockage test model (Fig. 8a) was built. The necessity of checking the operation of the tunnel with a large model (28% blockage ratio based on projected area/nozzle exit area) and combustion presented the first opportunity to determine the durability of the leading-edge structure as well as an approximate picture of the flowfield discussed in the preceding analytical section. This model is uncooled except at the leading edges where 0.051-in.-o.d., 0.005-in.-wall nickel tubes are brazed to the model parts. Figure 8b shows the blockage test model mounted in the tunnel.

During the blockage tests it was found that the integrity of the leading-edge tube can be maintained with water cooling even if the tube is slightly deformed by particles in the airstream as shown in Fig. 9a. However, if the particles have sufficient momentum to pierce the tube, the back pressure and flow rate cannot be maintained and the tube will overheat. For example, in a run which was prematurely stopped by an arc blowout the resulting damage to the compression ramp leading edge is shown in Fig. 9b. Upon inspection of the test setup a short piece of steel arc starting wire was found in the test cabin, indicating that when the arc was fired the starting wire connecting the electrodes was not vaporized completely in the arc chamber but instead was carried through the tunnel by the flowing gas. This wire apparently struck and perforated the 0.005-in.-thick tube slightly to the right of the ramp centerline. The coolant was thus free to discharge through the perforation and consequently starve the tube downstream which rapidly heated up, causing the braze bond to loosen and the tube to deform and eventually separate from the ramp. The tube upstream of the per-

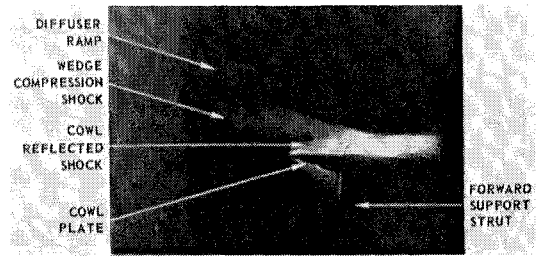

Fig. 10 Direct luminosity photograph of inlet flowfield without fuel injection.

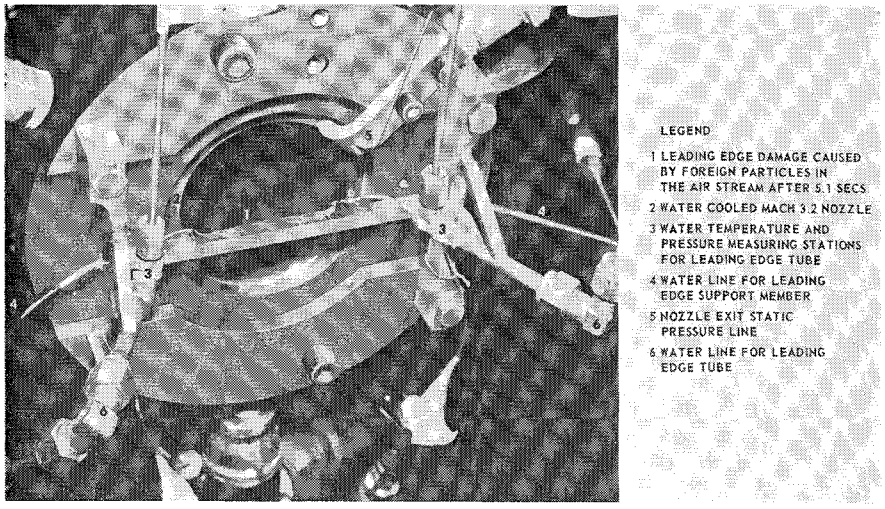

Fig. 11 View of 0.025-in.-radius leading edge after run at Mach 3.2 showing damage caused by failure of piping section upstream of nozzle.

foration would probably overheat at a slower rate and eventually separate from the ramp, since the back pressure on the tube dropped from 100 psia to about 5.4 psia. The drop in pressure would correspondingly drop the saturation temperature from 328° to 166°F which would more than offset the slight effect of the increased velocity.

Direct luminosity movies of the cowl area were taken during the blockage tests to show the inlet wave structure. Figure 10, an enlargement of one frame, shows the second wedge compression shock (θ_2 in Fig. 1) and the cowl-reflected shock (θ_3 in Fig. 1). The luminosity behind the first wedge shock is not great enough to be visible against the background. The second wedge compression shock appears to be positioned properly to intersect the cowl as desired. However, the cowl-reflected shock appears to strike the compression ramp slightly upstream of the designed cornerline causing a slightly overcompressed region, which in turn is followed by an expansion at the ramp corner where the flow enters the diverging combustion chamber. The displacement of the cowl-reflected shock may be due to a strong shock-boundary-layer interaction at the cornerline or to geometrical distortion of the model during testing. To compensate for errors in the position of the shocks in the flowfield, provisions for adjustment of the relative positions of the compression ramp, cowl leading edge and combustor walls with the fully cooled model are found to be definitely desirable.

Since the previously described work demonstrated the durability of the actively cooled 0.0255-in.-radius × 0.005-in.-wall leading-edge tube, there remained to be checked the approximate heat-transfer analysis previously described as well as the demonstration of the concept of the electroplated edge assembly. This experiment is most simply done in the APL arc-powered Mach 3.2 free jet tunnel where a much shorter edge can be used because the exit diameter of the nozzle is 2.74 in. Also, the necessary heat-transfer instrumentation can be isolated from the nozzle jet.

Two leading-edge models were built for test in the Mach 3.2 free jet. The first consisted of a single 0.0255-in.-radius × 0.005-in.-wall Ni 270 tube brazed to a water-cooled support member to permit checkout of the tunnel conditions and instrumentation. The second was an electroplated structure that included three 0.051-in.-o.d. Ni 270 tubes attached to a water-cooled support. These two models had total wedge angles of 35° and were mounted such that one surface was aligned with the airflow.

The single-tube model remained intact for 5.1 sec, at which time a section of piping upstream of the nozzle failed. Figure 11, taken after the run, shows the resultant destruction of the leading edge. Prior to the failure of the tube, steady-state heat-transfer data were obtained. Plenum conditions were p_t = 435 psia and h_t = 1195 Btu/lb. Pitot pressure measurements at the nozzle exit verified Mach 3.2 tunnel flow. The water flow rate was 0.057 lb/sec, and the corresponding temperature rise was 57°. These measurements lead to a q_s/A value of 10.9 Btu/sec-in^2 and a wall temperature of 716°R. For these conditions the Detra and Hidalgo expression indicates q_s/A = 7.91 Btu/sec-in^2 or 73% of the measured rate.

In Fig. 12a, a completed three-tube leading-edge assembly is shown in position at the exit of the Mach 3.2 nozzle. At

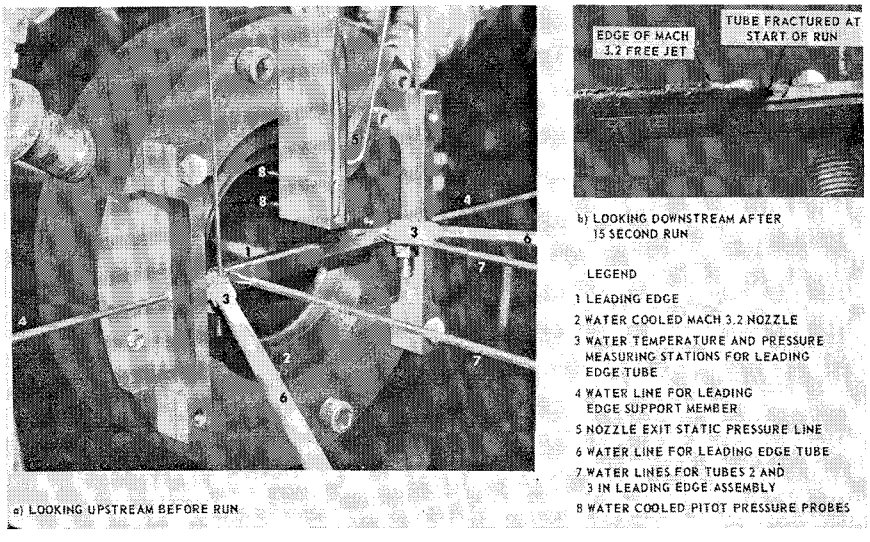

Fig. 12 Views of three 0.051-in.-o.d. tube leading-edge assembly before and after test at Mach 3.2.

the start of the run the leading-edge tube was fractured at the water inlet connection immediately dropping the water pressure in the tube to zero. The test, at $p_t = 442$ psia and $h_t = 1310$ Btu/lb, was continued for 15 sec to determine the durability of the edge assembly. Figure 12b shows a close-up view of the leading edge after the run. Leading-edge failure is restricted to the stagnation region. The integrity of the remaining structure is maintained by the coolant flowing through the second tube. This result demonstrates a significant benefit of the multi-tube leading-edge design, namely, damage to the leading-edge tube merely shifts the leading edge downstream approximately one tube diameter (in this case, ~0.050 in.). In an integrated inlet-combustor wind-tunnel model, e.g., Figs. 1 and 8, the damage would not cause significant changes in the flowfield or combustor test results.

Before concluding, a brief description of the techniques used during fabrication of the edge assemblies will be given. Figure 13a schematically illustrates the plating and machining jigs used to minimize the machining required for the edge assembly. During plating the tubes are held in tension to maintain straightness. The stagnation line on the leading tube is masked to prevent plating buildup in this region and to provide a reference surface for subsequent machining operations. The tongue section of the jig allows the plated nickel to form the shape required for attachment to the body of the model without machining in this region. After the wedge surfaces on the leading edge are machined, the tongue jig is removed and the edge assembly is brazed to the main body of the model as presented in Fig. 13b.

Figure 14a shows a three-tube assembly for the Mach 3.2 test after it has been electroplated and partially machined. Figure 14b shows a fully machined nickel leading-edge assembly containing seventeen 0.051-in.-o.d. Ni 270 tubes.

Because the success of the tube assembly is dependent upon a relatively high thermal conductivity, it is important to secure a high-quality deposition of plated nickel onto the nickel tubes. Figure 15 shows two photomicrographs of sections through joining regions. In part a) there is a region approximately 4 grain boundaries in width between a tube and the plated nickel. The thermal conductivity would be lower than nickel with this poor bond. Moreover, if plating solution is trapped in the bond region and then changes state during heating in the tunnel, an increase in volume may cause excessive distortions in the vicinity of the leading edge. By using careful plating techniques the plated nickel can be attached within 1 grain boundary of the tube as seen in part b).

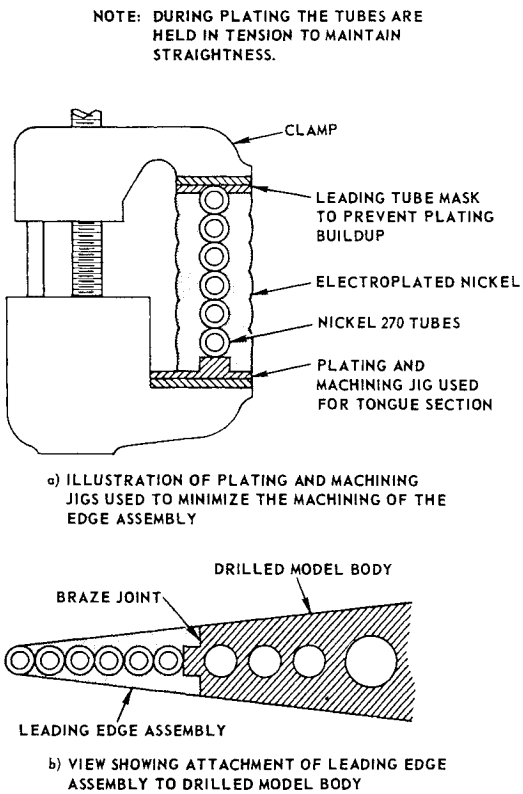

Fig. 13 Schematic views of plating jigs and attachment of leading-edge assembly to drilled model body.

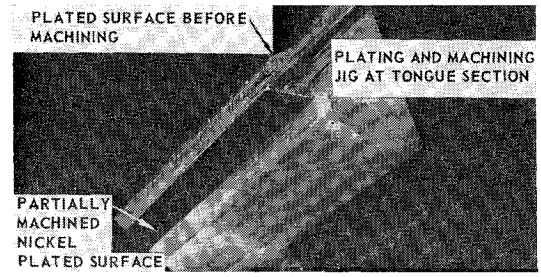

a) View of leading-edge assembly after it has been electroplated and partially machined

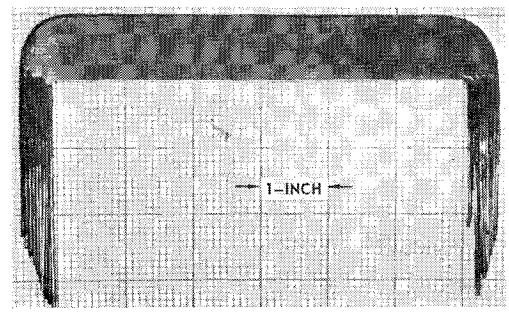

b) Electroplated nickel leading edge containing seventeen 0.041-in.-i.d. nickel tubes

Fig. 14 Fabrication photographs of nickel leading-edge assemblies.

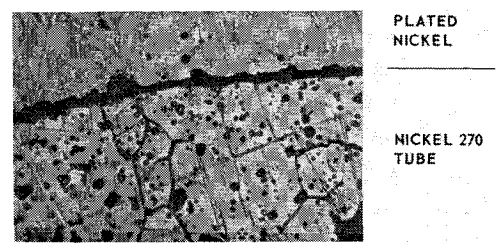

a) View of nickel tube with undesirable void between tube and plated nickel

b) View of nickel tube with satisfactory bond between tube and plated nickel

Fig. 15 Photomicrographs of Ni 270 tube and electroplated nickel interfaces.

Conclusions

The results of tests demonstrate the feasibility of a small-diameter, actively cooled leading-edge structure. Conventional heat-transfer and pressure drop expressions appear to be adequate for designing actively cooled leading-edge structures in the hypersonic environment. Although the construction of the structure requires rigorous control, it is practical. The incorporation of this concept into vehicle design should permit significant increases to be made in the permissible hypersonic velocity-altitude operating environment.

References

[1] Bowers, D. A., "Leading Edges Development-Dyna Soar," Rept. D2 80085, June 26, 1963, The Boeing Co., Seattle, Wash.

[2] Scala, S. M. and Nolan, E. J., "Aerothermodynamic Feasibility of Graphite for Hypersonic Glide Vehicles," Report TIS R60SD425, Aug. 2, 1960, General Electric Co., Space Sciences Lab., Philadelphia, Pa.

[3] Jorgensen, L. H. and Baum, G. M., "Charts for Equilibrium Flow Properties of Air in Hypervelocity Nozzles," TN D-1333, Sept. 1962, NASA.

[4] Detra, R. W. and Hidalgo, H., "Generalized Heat Transfer Formulae and Graphs," Rept. 72, March 1960, Avco-Everett Research Lab., Everett, Mass.

[5] Lees, L., "Laminar Heat Transfer over Blunt-Nosed Bodies at Hypersonic Flight Speeds," *Jet Propulsion*, Vol. 26, 1956, pp. 259–274.

[6] "Materials in Design Engineering/Materials Selector Reference Issue," Reinhold, New York, mid-October 1959, Vol. 50, No. 5, pp. 13, 24, 25, 61.

[7] "Nickel 270 Basic Data," The International Nickel Co. Inc., Huntington, W. Va.

[8] Marks, L. S., *Mechanical Engineers Handbook*, 5th ed., McGraw-Hill, New York, 1951.

[9] Timoshenko, S., *Strength of Materials*, 3rd ed., Pt. II, Van Nostrand, Princeton, N.J., 1957, Chap. VI, p. 232.

[10] Wilson, R. E., "Handbook of Supersonic Aerodynamics-Viscosity and Heat Transfer Effects," Rept. 1488, 5, Aug. 1, 1966, U.S. Naval Ordnance Lab., White Oak, Md.

[11] Billig, F. S., "Shock-Wave Shapes around Spherical- and Cylindrical-Nosed Bodies," *Journal of Spacecraft and Rockets*, Vol. 4, No. 6, June 1967, pp. 822–823.

[12] Ambrosio, A. and Wortman, A., "Stagnation Point Shock Detachment Distance for Flow Around Spheres and Cylinders," *ARS Journal*, Vol. 32, No. 2, Feb. 1962, p. 281.

[13] Gunther, F. C., "Photographic Study of Surface-Boiling Heat Transfer to Water with Forced Convection," *Transactions of the American Society of Mechanical Engineers*, Vol. 73, 1951, pp. 115–123.